Conserved core of amyloid fibrils of wild type and A30P mutant α-synuclein

Min-Kyu Cho,[1] Hai-Young Kim,[1] Claudio O. Fernandez,[2] Stefan Becker,[1] and Markus Zweckstetter[1,3]*

[1]Department for NMR based Structural Biology, Max Planck Institute for Biophysical Chemistry, D-37077, Goettingen, Germany

[2]Instituto de Biología Molecular y Celular de Rosario, Universidad Nacional de Rosario, Suipacha 531, S2002LRK Rosario, Argentina

[3]DFG Research Center for the Molecular Physiology of the Brain (CMPB), Göttingen, Germany

Received 1 October 2010; Revised 23 November 2010; Accepted 26 November 2010
DOI: 10.1002/pro.570
Published online 8 December 2010 proteinscience.org

Abstract: The major component of neural inclusions that are the pathological hallmark of Parkinson's disease are amyloid fibrils of the protein α-synuclein (aS). Here we investigated if the disease-related mutation A30P not only modulates the kinetics of aS aggregation, but also alters the structure of amyloid fibrils. To this end we optimized the method of quenched hydrogen/deuterium exchange coupled to NMR spectroscopy and performed two-dimensional proton-detected high-resolution magic angle spinning experiments. The combined data indicate that the A30P mutation does not cause changes in the number, location and overall arrangement of β-strands in amyloid fibrils of aS. At the same time, several residues within the fibrillar core retain nano-second dynamics. We conclude that the increased pathogenicity related to the familial A30P mutation is unlikely to be caused by a mutation-induced change in the conformation of aS aggregates.

Keywords: α-synuclein; NMR spectroscopy; structure; amyloid fibril; mutation

Introduction

The pathological hallmark of Parkinson's disease (PD) and several other neurodegenerative disorders is the deposition of intracytoplasmic neuronal inclusions termed Lewy bodies.[1] The major components of Lewy bodies are amyloid fibrils of the protein α-synuclein (aS).[2] Three separate mutations (A30P, E46K, and A53T) as well as duplications or triplications of the aS gene, which increase levels of aS with no alteration in sequence, cause PD.[3–5] While dopaminergic nerve cell loss clearly is linked to enhanced aS aggregation, oligomeric intermediates might be the most toxic species.[6] However, due to their transient and heterogeneous nature they are difficult to characterize.[7,8]

Since their discovery, the three disease-related aS mutants have been the subject of intense study, as differences in aggregation behavior and morphology with respect to the wild-type (*wt*) form may yield valuable insights into the fundamental processes underlying amyloidogenic diseases.[3,9–24] As in the case of *wt* aS, all three mutants are natively unfolded in aqueous solution,[20] although the propensities for residual secondary and tertiary structure are slightly altered.[9,17,21,25,26] Upon binding to micelles or small unilamellar vesicles, the N-terminal domain of aS assumes a helical structure, with a reduced affinity for A30P aS.[22,27–29] In agreement with the aggregation of aS into fibrillar Lewy bodies, the A53T and

Abbreviations aS, α-synuclein; GuSCN, Guanidine thiocyanide; H/D exchange, hydrogen/deuterium exchange; HR-MAS, high-resolution magic angle spinning; HSQC, heteronuclear single quantum correlation; NMR, nuclear magnetic resonance; PD, Parkinson's disease; wt, wild type

Grant sponsor: Max Planck Society; Grant Sponsor: Alexander von Humboldt Foundation; Grant Sponsor: BMBF; Grant number: NGFN-Plus 01GS08190; Grant sponsor: European Union; Grant number: NEURASYNC PITN-GA-2009-238316; Grant sponsor: DFG Heisenberg scholarship; Grant number: ZW 71/2-1 and 3-1.

**Correspondence to:* Markus Zweckstetter, Department for NMR-based Structural Biology, Max Planck Institute for Biophysical Chemistry, Am Fassberg 11, 37077 Göttingen, Germany. E-mail: mzwecks@gwdg.de

E46K mutations have an increased aggregation propensity *in vitro*. In contrast, contradicting observations regarding oligomerization and aggregation kinetics were reported for the A30P mutant.[12,15,20,21]

The secondary structure of amyloid fibrils of *wt* aS has been studied by a battery of biophysical techniques, including hydrogen/deuterium exchange measurements coupled to solution-state nuclear magnetic resonance (NMR) spectroscopy,[30] solid state NMR spectroscopy,[30–32] mass spectrometry,[33] and electron paramagnetic resonance spectroscopy.[34] The combined data indicate that the rigid core of amyloid fibrils of aS starts at about residue 38 and ends at about residue 100, and comprises a minimum of four β-strands.

Much less is known about the structural properties of amyloid fibrils formed by the disease-related mutants of aS. According to electron microscopy and atomic force microscopy A30P and A53T aS possess similar fibril morphology with some deviations in the degree of twist along the fibrillar axis.[23] A recent solid-state NMR study on amyloid fibrils of A53T aS suggested that the fibrillar core of A53T aS is extended by about five residues when compared to the wild-type protein,[19] in agreement with the higher aggregation rate of A53T aS.

Here we compare the conformational properties of amyloid fibrils of *wt* and A30P mutant aS using a combination of hydrogen/deuterium (H/D) exchange[35] and high-resolution magic angle spinning (HR-MAS) in combination with liquid-state NMR spectroscopy.[36] Our data demonstrate that the fibrillar core of aS is not perturbed by the genetic mutation A30P.

Results and Discussion

Flexible regions in amyloid fibrils of αS detected by HR-MAS NMR spectroscopy

^{15}N isotope labeled *wt* and A30P aS were aggregated at 37°C for 7 days with agitation. Electron microscopy showed a morphology that is characteristic for amyloid fibrils [Fig. 1(b)]. Initially, a conventional one-dimensional liquid-state NMR spectrum was measured. Only signal from water was detected, demonstrating that the concentration of monomeric aS is below the detection limit. In addition, after the NMR measurements (see below) the sample was centrifuged and a ^{1}H spectrum of the supernatant was recorded. Despite 1024 scans, no protein signals were detected in the spectrum (data not shown). Signals from aggregates are not expected to be seen due to their reduced mobility, slow rotational diffusion and associated variations in magnetic susceptibility anisotropy. To overcome the broadening due to variations in magnetic susceptibility anisotropy, we applied high-resolution magic angle spinning.[36]

Narrow ^{1}H line widths obtained under HR-MAS allowed measurement of a ^{1}H,^{15}N heteronuclear single quantum coherence (HSQC) spectrum. The 2D spectrum showed a narrow dispersion of peaks [Fig. 1(c)], indicating the absence of rigid secondary and tertiary structure. Comparison with the ^{1}H,^{15}N-HSQC of monomeric aS, revealed that many cross peaks in the two spectra overlap. We assigned all peaks in the HR-MAS spectrum, which deviated by less than 0.2 ppm for ^{15}N and less than 0.02 ppm for ^{1}H from a single cross-peak in the HSQC of monomeric aS, to the corresponding residue [Fig. 1(c,d)]. Based on this approach, signals of 28 residues in the region 98–140 could be identified [Fig. 1(d)]. The C-terminal domain was previously suggested to be dynamically disordered, however, due to larger line-width and lower sensitivity of carbon-carbon correlation spectra only a few of the residues in the C-terminal domain could be assigned by solid-state NMR.[30,31,33] Sequence-specific assignment of residues in the C-terminal domain of aS fibrils is important for evaluation of the effect of post-translational modifications in the fibrillar state, such as phosphorylation at S129 and nitration at Y125, Y133, and Y136.[37,38] In addition a few signals were observed in the HR-MAS spectrum, which overlapped with signals of residues 1-98 of monomeric aS, for example residues 45, 47, 82–83, and 89 [Fig. 1(c)]. Based on chemical shift similarity [Fig. 1(d)] these residues are thus tentatively assigned to the core of aS fibrils, suggesting the presence of dynamics in the fibrillar core of aS amyloid. Note that due to the high molecular weight of amyloid fibrils rigid residues are not expected to be observed by liquid-state NMR in agreement with the absence of most of the signals from the fibrillar core in the HR-MAS spectra. To make these signals observable in ^{1}H,^{15}N HSQC spectra the corresponding residues must be flexible on fast time scales including the pico and nano-second time scale.

Optimized method for hydrogen/deuterium exchange coupled to NMR spectroscopy

H/D exchange combined with NMR spectroscopy has been widely used for the study of protein folding and for the characterization of the structure of protein aggregates.[39–43] The large size of amyloid fibrils hampers direct detection of H/D exchange in amyloid fibrils by solution-state NMR spectroscopy. Hence, a critical step has been introduced that is rapid dissociation of fibrils into unfolded protein during, which the H/D exchange information of the fibrillar state is preserved. Deuterated dimethyl sulfoxide with 5% H_2O[39,42] or 100 m*M* of deuterated SDS, pD 3.5 in 100% D_2O[43] or 6*M* guanidine thiocyanide (GuSCN), 0.4% formic acid (pD 2.4) in 99.9% D_2O[33] are the solvents used for that purpose. Typically, a series of aliquots from a solution containing fibrils are subjected to different durations of H/D exchange (denoted as forward exchange) followed by lyophilization. Then the fibrils are dissociated in the dissolving solution in the NMR spectrometer and a series of ^{15}N—^{1}H spectra are measured,

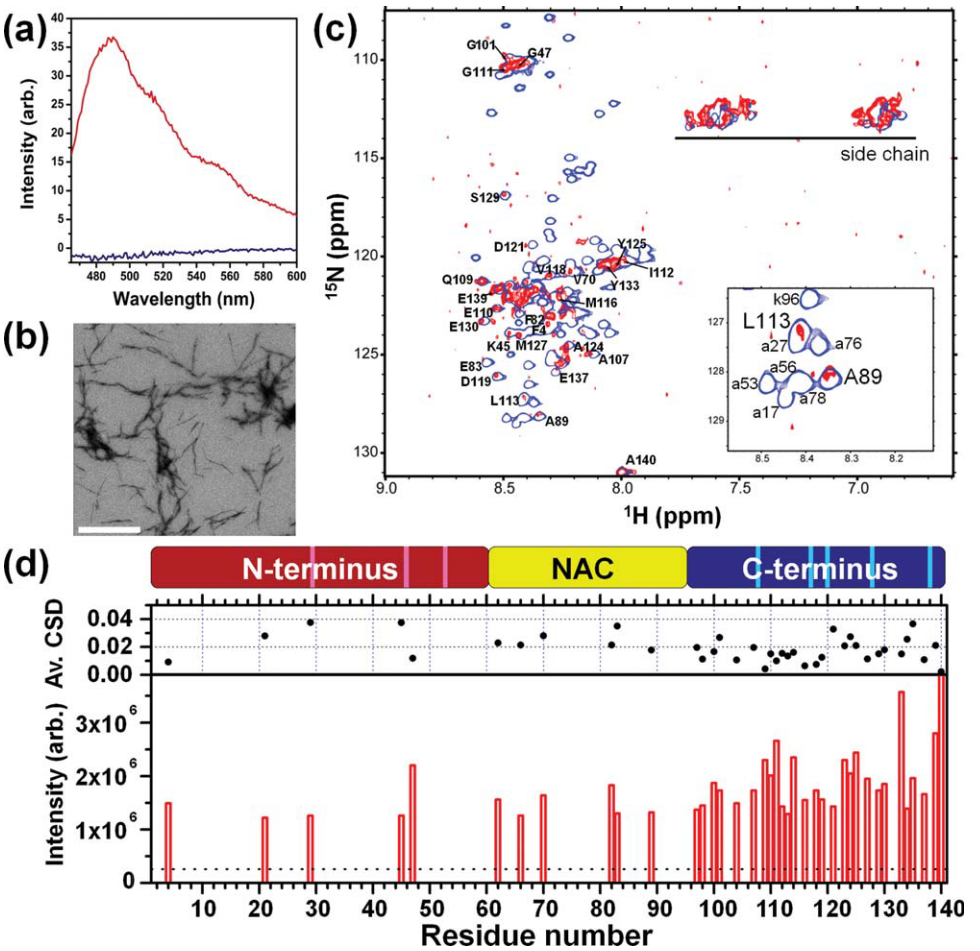

Figure 1. NMR-based detection of residues with nano-second dynamics in amyloid fibrils of aS. (**a**) Thioflavin T fluorescence of amyloid fibrils (red) of wt aS and of monomeric aS (blue). (**b**) Electron migrograph of aS fibrils that were used in HR-MAS NMR measurements. (**c**) Comparison of 2D ^{15}N-^{1}H HSQC spectra observed for fibrillar aS using HR-MAS (red) and monomeric wt aS (blue). (**d**) Residue specific peak intensities observed in the ^{15}N—^{1}H HR-MAS HSQC spectrum of amyloid fibrils of wt aS shown in Figure 1(c). The dashed line indicates the noise level in the spectrum representing the error of the shown peak intensities. Note that for most residues in the N-terminal region from residue 1–98 no signal at the position expected for monomeric aS was found, demonstrating that the concentration of residual monomeric protein is below detection level. On top the domain organization of aS is shown. The three sites affected by disease-associated mutation (A30P, E46K, A53T) are indicated in magenta. The five prolines of aS are marked in cyan. In addition, averaged ^{15}N, ^{1}H chemical shift differences between fibril and monomer, calculated according to $[(\Delta N/5)^2+\Delta H^2]^{0.5}$, are depicted.

in which the decay of cross-peaks is followed. For determination of protection factors, often a single HSQC recorded at a specific time point during back-exchange is used. Cross-peak intensities in HSQC spectra obtained for aliquots with different H/D exchange times are then compared to those of an external reference (often amyloid fibrils without H/D exchange) and are fitted to a single exponential curve as a function of H/D exchange time. Some of the H/D exchange experiments require several months due to the highly stable cross-β structure of amyloid fibrils.[30]

We modified this method to reduce the amount of required material and to more easily distinguish exposed and buried residues. The main modification is the use of a 50%/50% H_2O/D_2O solution with 2*M* GuSCN, 0.4% formic acid, pD 2.4. As a mixture of 50% D_2O and 50% H_2O is used, the final peak intensity in the HSQC after reaching equilibrium should be 50% of the total amount of monomeric protein in the solution. Thus, the initial peak intensity ratio (at time 0 in the dissolving buffer, I_{1wEX}/I_{noEX}) can be obtained by extrapolation of a simple exponential decay curve with 0.5 offset. When this method is applied to fibrils, which had been subjected to H/D exchange, the initial peak intensity should report on the reduced amount of hydrogens in the fibril. The use of the internal reference intensity as proposed here can minimize possible experimental errors that may be introduced by unequal amounts of amyloid fibrils, when the H/D exchange is probed with multiple samples. Moreover, residues for which amide protons were exchanged by more than 50% show an increase in protonation during the back-exchange

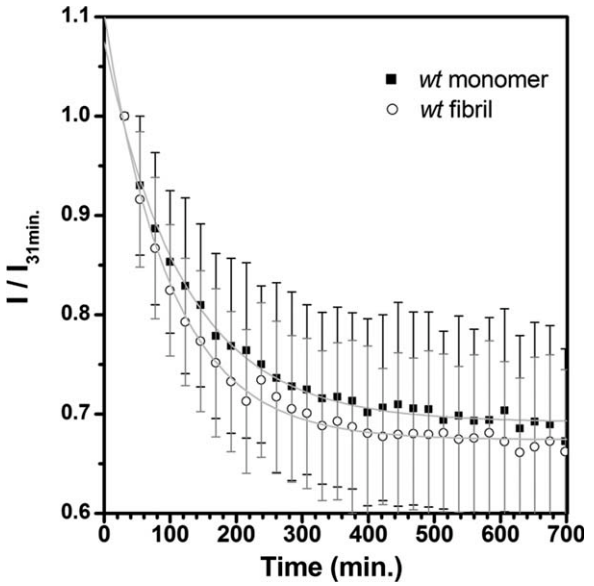

Figure 2. Decay of signal intensity observed in dissolving buffer for amyloid fibrils (open circles) and monomeric aS (filled squares) due to exchange with buffer. Both the amyloid fibrils and the monomeric protein were fully protonated prior to dissolving. The dissolving buffer consists of a 50%/50% H_2O/D_2O solution with 2*M* GuSCN, 0.4% formic acid, pD 2.4. Shown are average values obtained by averaging over all signals observed for backbone amide protons in a series of 2D $^{1}H—^{15}N$ HSQC spectra and normalizing it by the intensity (I_{31min}) observed in the first HSQC spectrum, which was recorded within 31 minutes after the start of the dissolving procedure.

period, resulting in a clear distinction between strongly buried (slower H/D exchange) and exposed (faster H/D exchange) residues from a single H/D exchange experiment. The method was tested with fully protonated monomeric and fibrillar *wt* aS. Figure 2 shows a comparison of the development of NMR signal intensities for monomeric and fibrillar aS during back exchange. The average decay curves follow a single exponential. No significant difference was observed between monomeric and fibrillar aS indicating that dissociation of fibrils in 2*M* GuSCN is very rapid. H/D back-exchange is already occuring during the first HSQC spectrum (acquired within 31 minutes after mixing the solution and the protein); hence the ratio of cross-peak intensities between the HSQC at equilibrium and that in the first HSQC after dissolving is not 0.5 but 0.7. The data demonstrate that amyloid fibrils of aS are rapidly dissociated and that the back-exchange is sufficiently slow to be followed by two-dimensional NMR spectroscopy.

Back-exchange profiles of one week H/D exchanged fibrils of wt *and A30P aS*

wt and A30P aS fibrils were prepared and resuspended in 99.9% D_2O with 0.1% formic acid, pD 4. After one week of H/D exchange at 4°C, the fibrils were collected by ultracentrifugation, resuspended into the dissolving buffer and protonation levels were followed by a series of 2D $^{15}N—^{1}H$ HSQC spectra. Peak intensity ratios shown in Figure 3 (a) were calculated based on the peak intensities observed in the first $^{15}N—^{1}H$ HSQC ($I_{31mn.}$) spectrum. For residues 1–37 in the N-terminal domain and 98–140 at the C-terminus, peak intensity ratios increased by more than 50%. Increasing peak intensities during back-exchange report on increasing levels of protonation, indicating that these residues had exchanged more than 50% of their protons during the forward exchange period. Conversely, cross-peak intensities of residues L38 to K97 showed a much smaller increase in peak intensities, 40% or less, or even showed decreasing peak intensities, indicating that the central domain of aS fibrils is more solvent protected. Some differences were observed between the back-exchange curves of *wt* and A30P aS, in particular in the final value of peak intensity ratio after complete back-exchange [Fig. 3(a)]. As the peak intensity ratios report on the variation of protonation levels relative to the intensity observed in the initial HSQC, the differences might point to differences in the solvent protection in the fibrillar state. Differences in the conformation present in the denaturing buffer, which might also affect the back-exchange, are unlikely to significantly contribute as the rates of back-exchange are very similar for residues in *wt* and A30P aS.

A conserved solvent protected core in amyloid fibrils of wt *and A30P aS*

The peak intensity ratio, which is calculated for the time point zero of back-exchange from the back-exchange curve, represents the ratio of remaining hydrogens in amyloid fibrils after one week of H/D exchange (I_{1wEX}/I_{noEX}). Figure 3(b) shows the back-calculated intensity ratios at time point zero for fibrils of *wt* and A30P aS, which had been exposed to H/D exchange for seven days. Two clearly distinct regions can be identified in both *wt* and A30P aS: residues M1-V37 and K98-A140 have deuterium incorporation levels of 59–90%. In contrast, for residues L38-K97 less than 60% of amide protons have exchanged, indicating that residues 38–97 are more solvent protected in the fibrillar state. In wt aS, the N— and C-terminal domains have average deuterium incorporation levels of 0.73+/−0.06 and 0.76+/−.07, respectively. The C-terminal domain is most strongly affected by solvent exchange, in agreement with its detection in the HR-MAS spectra (Figs. 1 and 3). Variations in the deuterium incorporation levels within the flanking domains can be caused by the presence of residual structure, in particular in the N-terminal domain that is not observed in the HR-MAS spectra and thus has only limited motion on the nano-second time scale. In the C-terminal domain residual structure might be

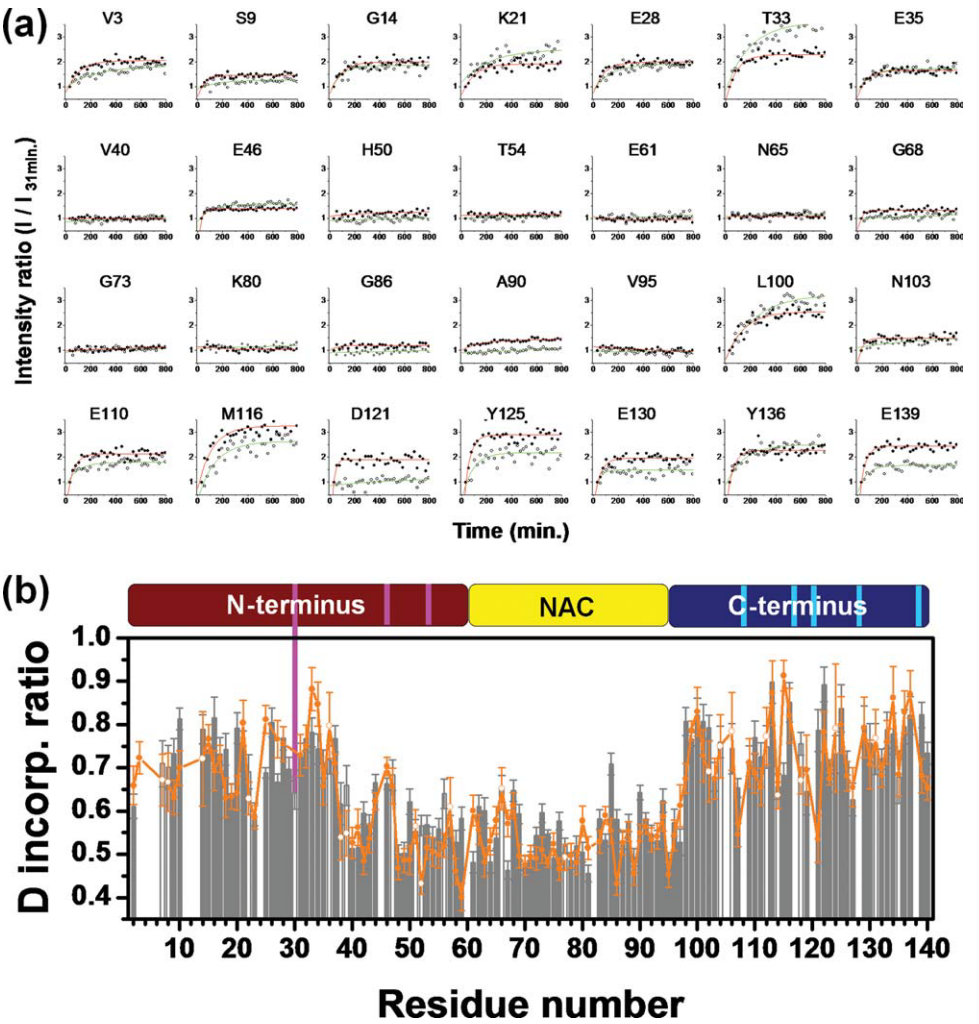

Figure 3. Back-exchange profiles of one week H/D exchanged fibrils of wt and A30P aS. The back-exchange buffer was a 50%/50% H_2O/D_2O solution with 2*M* GuSCN, 0.4% formic acid, pD 2.4. The temperature was 4°C. (a) Residue-specific changes in peak intensities observed for wt (filled circles) and A30P (open circles) aS during back-exchange. Each back-exchange profile was fit with a single exponential curve (red, wt αS; green, A30P αS) reporting on the kinetics of back-exchange. (b) Levels of deuterium incorporation in amyloid fibrils of wt (gray) and A30P (orange) aS after one week of H/D exchange at 4°C, pD 4.0. Levels of deuterium incorporation are equal to the peak intensity ratio that is back-calculated for time point zero of back-exchange from the back-exchange curves and takes into account that after completion of the back-exchange the protonation level is 50%. Error bars were calculated on the basis of the signal-to-noise ratio in the last and first HSQC spectrum. Residues of wt aS with partial signal overlap are shown with open bars. The three sites affected by disease-associated mutation (A30P, E46K, A53T) are indicated in magenta. The five prolines of aS are marked in cyan.

promoted by the presence of the five proline residues [indicated in cyan in Fig. 3(b)]. Particularly striking are the sharp boundaries in the solvent protection map observed at residues 37–38 and 97–98. The higher solvent protection for residues L38-K97, is in agreement with a protease resistant core of aS fibrils comprising residues 31–101,[44] previous hydrogen exchange experiments coupled to mass spectrometry (residues 39–101)[33] or solution-state NMR (residues 35–96)[30] and EPR studies on site-directed spin-labeled aS fibrils, which revealed a well-ordered central region (residues 34–101) with parallel, in-register β-strands.[45]

Our data demonstrate that the overall pattern of deuterium incorporation in amyloid fibrils of *wt* and A30P aS is very similar in the solvent protected central domain as well as in the more exposed N- and C-terminal domains [Fig. 3(b)]. Most differences are within the experimental errors. Slightly outside the experimental errors, are the differences between the levels of protonation of A30P and *wt* aS close to the site of mutation potentially induced by minor changes in local conformation. Importantly, the sharp boundaries between the two domains are highly conserved, suggesting that the A30P mutation does not change the size of the monomeric core of aS fibrils. This is in contrast to the genetic mutation A53T, which according to solid-state NMR spectroscopy, causes an extended boundary of the fibrillar region in A53T aS (residue number 38–100)

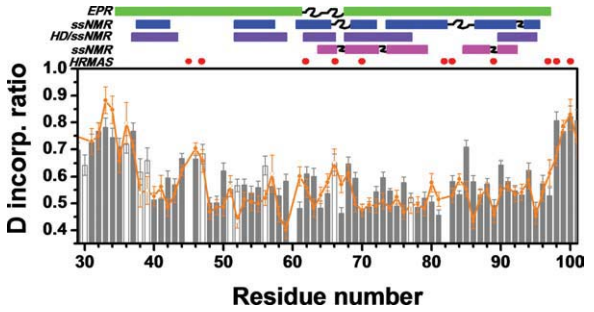

Figure 4. The conserved solvent protected core in amyloid fibrils of wt and A30P aS. Deuterium incorporation levels in the fibrillar core of wt (gray bar) and A30P (orange circle) aS (taken from Fig. 3) are compared to previous results for wt aS fibrils using electron paramagnetic resonance[34] (green) and solid-state NMR (blue, Heise *et al*.[31]; purple, Vilar *et al*.[30]; pink, Kloepper[46]). Red circles mark the location of residues observed by HR-MAS and tentatively assigned to the fibrillar core (Fig. 1).

compared to *wt* aS (position 38–95).[19] Thus, the two genetic mutations A30P and A53T aS might differentially affect the structure of aS aggregates. At the same time, it should be noted that the length of the fibrillar core varies slightly in several investigations even for *wt* aS.[30,31,33,34,46] These variations might be related to the polymorphic nature of amyloid fibrils and the strong influence of solution conditions on the kinetics of aggregation.

The core of amyloid fibrils of wt *and A30P aS*

Are there differences in structure between *wt* and A30P aS fibrils within the 38–97 region? Figure 4 shows a comparison of the deuterium incorporation levels in detail. For both proteins a first dip in the profile of deuterium incorporation is seen for residues L38-K43, which is clearly separated from the remainder of the fibrillar core by the more solvent exposed residues 44–47. Taking into account that it is well established that aS fibrils are composed of β-sheets, the H/D exchange data suggest that residues L38-K43 form a β-strand. The higher levels of deuterium incorporation downstream indicate that residues T44-G47 form a turn or loop in both *wt* and A30P aS amyloid fibrils, in agreement with the observation of signals for T44 and E46 in the HR-MAS spectra (Figs. 1 and 4). Importantly, the third known familial mutation E46K is located in this loop (Fig. 3). The loop is followed by the residue stretch V48-N65, which shows lower levels of deuterium incorporation pointing to the presence of hydrogen-bonded β-structure. At the same time, however, there is some variation in the levels of deuterium incorporation in this region, potentially caused by the presence of shorter elements of β-structure. In both A30P and *wt* aS, this region ends at V66-G68, a residue stretch, which is more solvent exposed (Fig. 4), which gives rise to a signal in the $^{15}N—^{1}H$ HR-MAS spectrum (Fig. 1) and which was previously implicated in turn formation in amyloid fibrils of aS.[30,31,46] The most solvent protected region is V70-Q79 (Fig. 4). Within this region, there might be some differences in the level of deuterium incorporation between A30P and *wt* aS, e.g., at G73. The remainder of the fibrillar core region up to K97 has then again slightly increased levels of deuterium incorporation in both *wt* and A30P aS. The combined data demonstrate that the solvent protection profiles in the flanking domains as well as in the fibrillar core are highly similar for A30P and *wt* aS. We attribute minor differences between the two profiles to small conformational differences, unavoidable variations in aggregation and the polymorphic nature of amyloid fibrils.[30,31,46]

Interestingly, the levels of deuterium incorporation are not uniform across the fibrillar core for both proteins. Primary factors that contribute to solvent exchange are hydrogen bonding and burial within the overall structure. It was previously shown that several regions in aS fibrils, for example residues V70-Q79 and residues G86-I88, have β-structure and are thus likely to be involved in hydrogen bonds,[30,31,46] suggesting that the differences in the average levels of deuterium incorporation in these regions are due to different degrees of burial in the amyloid fibrils. Average deuterium levels for residues 38–43, 48–65, 70–79, 86–97 in *wt* aS fibrils are 0.58, 0.56, 0.52, and 0.56, respectively, suggesting (also the standard deviation of +/−0.06 is quite large) that residues V70-Q79 are the most buried part of aS. Residues V70-Q79 form the most hydrophobic region of aS and are part of the 12 residue stretch that is essential for aggregation of aS,[47–49] suggesting that residues, which are important for conversion of aS from a monomeric into an aggregated state also form the core in the structure of amyloid fibrils. Moreover, as the variations in the solvent protection for different regions with β-structure are highly similar in A30P and *wt* aS, changes in the overall arrangement of the β-strands induced by the A30P mutation are unlikely.

Conclusions

The aim of this study was to investigate if the pathogenic mutation A30P not only modulates the kinetics of aS aggregation, but also alters the structure of amyloid fibrils, which form the end stage of aggregation and the histopathological hallmark of Parkinson's disease. To this end we developed an optimized method for H/D exchange of amyloid fibrils and combined it with two-dimensional proton-detected HR-MAS experiments. The HR-MAS measurements suggested that several residues within the fibrillar core, which most likely interconnect β-strands, retain nanosecond dynamics in the amyloid fibrils, supporting the idea that even the core of amyloid fibrils is

not a single rigid unit.[50] Comparison of solvent protection profiles for A30P and *wt* aS indicate that the A30P mutation does not cause changes in the number, location and overall arrangement of β-strands in amyloid fibrils of aS. This is in clear contrast to design mutations of aS, in which even a single proline substitution in the fibrillar core (A56P) strongly impairs both the kinetics of aggregation and the β-structure of insoluble aggregates.[51] Interestingly, whereas the design mutations with impaired β-structure result in strongly enhanced neurotoxicity in four different model systems for Parkinson's disease, conflicting results for the toxicity of A30P aS in model systems for Parkinson's disease exist.[52] We cannot exclude that there might be differences in the structure of amyloid fibrils prepared *in vitro* from those found in the brain of patients with Parkinson's disease. However, preparation of amyloid fibrils of wt and A30P mutant aS prepared *in vitro* enables a comparison of their structural properties under identical conditions (pH, buffer, cofactors), which is impossible for material extracted from the brain. In summary our data suggest that the increased pathogenity related to the familial A30P mutation is unlikely to be caused by a mutation-induced change in the conformation of aS aggregates.

Materials and Methods

^{15}N isotope labeled recombinant *wt* and A30P aS were expressed and purified from *E. Coli* as described previously.[9] Protein solutions were prepared in 20 m*M* Tris-HCl (pH 7.5 at 25°C), 100 m*M* NaCl and 0.02% NaN_3 with protein concentrations of $\sim$ 100 μ*M*. Fibrillization was achieved by incubation at 37°C for 7 days with agitation and monitored by a thioflavin T fluorescence assay [Fig. 1(a)] as described previously.[53] Fibrils were collected by two consecutive steps of centrifugation (215,000 g) and resuspension in distilled H_2O to remove residual monomeric protein and buffer. The final pellet was resuspended in 50 m*M* HEPES (pH 7.4), 100 m*M* NaCl solution for HR-MAS NMR measurements.

For electron microscopy, αS fibrils were prepared on a glow-discharged carbon foil and stained with 1 % uranyl acetate. The samples were evaluated with a CM 120 transmission electron microscope (FEI, The Netherlands). Images were taken with a 2048×2048 TemCam 224 A camera (TVIPS, Germany).

The optimized protocol for hydrogen-deuterium exchange is described in the main text. To slow down H/D exchange and in that way allow a better definition of regions with only slight differences in solvent protection,[33] the forward H/D exchange was done in 0.1% formic acid (pD 4.0), 200 m*M* NaCl in 99.9 % D_2O. The forward H/D exchange was stopped, fibrils were collected by ultracentrifugation, frozen by liquid nitrogen and stored in a refrigerator at −80°C. Note that monomers or oligomers that might dissociate from the fibrils during the 7 days of forward H/D exchange are usually not or only in very small concentrations found in the pellet after ultracentrifugation. Thus, they do not significantly influence the subsequent back-exchange curves. Subsequently, back-exchange in the dissolving buffer was followed by a series of 2D ^{1}H—^{15}N HSQC spectra recorded on a Bruker AVANCE 600 MHz NMR spectrometer equipped with a 5 mm triple-resonance, pulsed-field z-gradient cryoprobe. Preparative steps such as shimming and temperature equilibration resulted in a dead time of about 8 minutes before the start of the first HSQC. Acquired spectra were processed with linear prediction for the ^{15}N dimension and analyzed by NMRPipe.[54] Resonance assignments in the dissolving buffer were obtained with the help of a GuSCN titration and a 3D HNN experiment.[55]

HR-MAS spectra were recorded on a Bruker Avance 900 MHz spectrometer equipped with a 4 mm high-resolution MAS probe with the sample spinning at 7.2 kHz.

Acknowledgments

We thank Karin Giller for technical help, Dietmar Riedel for electron micrographs and Prof. Dr. Christian Griesinger for useful discussions.

References

1. Goedert M, Spillantini MG, Serpell LC, Berriman J, Smith MJ, Jakes R, and Crowther RA (2001) From genetics to pathology: tau and alpha-synuclein assemblies in neurodegenerative diseases. Philos Trans R Soc Lond B Biol Sci 356:213–227.
2. Spillantini MG, Schmidt ML, Lee VM, Trojanowski JQ, Jakes R, and Goedert M (1997) Alpha-synuclein in Lewy bodies. Nature 388:839–840.
3. Juan J.Zarranz JA (2004) The new mutation, E46K, of alpha-synuclein causes parkinson and Lewy body dementia. Annals of Neurology 55:164–173.
4. Polymeropoulos MH, Lavedan C, Leroy E, Ide SE, Dehejia A, Dutra A, Pike B, Root H, Rubenstein J, Boyer R, Stenroos ES, Chandrasekharappa S, Athanassiadou A, Papapetropoulos T, Johnson WG, Lazzarini AM, Duvoisin RC, Di Iorio G, Golbe LI, Nussbaum RL (1997) Mutation in the {alpha}-Synuclein Gene Identified in Families with Parkinson's Disease. Science 276: 2045–2047.
5. Singleton AB, Farrer M, Johnson J, Singleton A, Hague S, Kachergus J, Hulihan M, Peuralinna T, Dutra A, Nussbaum R, Lincoln S, Crawley A, Hanson M, Maraganore D, Adler C, Cookson MR, Muenter M, Baptista M, Miller D, Blancato J, Hardy J, Gwinn-Hardy K. (2003) alpha-Synuclein locus triplication causes Parkinson's disease. Science 302:841.
6. Lansbury PT, Lashuel HA (2006) A century-old debate on protein aggregation and neurodegeneration enters the clinic. Nature 443:774–779.
7. Lashuel HA, Lansbury PT, Jr. (2006) Are amyloid diseases caused by protein aggregates that mimic bacterial pore-forming toxins? Q Rev Biophys 39:167–201.

8. Kim HY, Cho MK, Kumar A, Maier E, Siebenhaar C, Becker S, Fernandez CO, Lashuel HA, Benz R, Lange A, Zweckstetter M (2009) Structural properties of pore-forming oligomers of alpha-synuclein. J Am Chem Soc 131:17482–17489.
9. Bertoncini CW, Fernandez CO, Griesinger C, Jovin TM, Zweckstetter M (2005) Familial mutants of alpha-synuclein with increased neurotoxicity have a destabilized conformation. J Biol Chem 280:30649–30652.
10. Bodner CR, Maltsev AS, Dobson CM, Bax A. Differential phospholipid binding of alpha-synuclein variants implicated in Parkinson's disease revealed by solution NMR spectroscopy. Biochemistry 49:862–871.
11. Bussell R, Jr., Eliezer D (2001) Residual structure and dynamics in Parkinson's disease-associated mutants of alpha-synuclein. J Biol Chem 276:45996–46003.
12. Choi W, Zibaee S, Jakes R, Serpell LC, Davletov B, Crowther RA, Goedert M (2004) Mutation E46K increases phospholipid binding and assembly into filaments of human alpha-synuclein. FEBS Lett 576:363–368.
13. Conway KA, Harper JD, Lansbury PT (1998) Accelerated in vitro fibril formation by a mutant alpha-synuclein linked to early-onset Parkinson disease. Nat Med 4:1318–1320.
14. Conway KA, Harper JD, and Lansbury PT, Jr (2000) Fibrils formed in vitro from alpha-synuclein and two mutant forms linked to Parkinson's disease are typical amyloid. Biochemistry 39:2552–2563.
15. Conway KA, Lee SJ, Rochet JC, Ding TT, Williamson RE, Lansbury PT, Jr (2000) Acceleration of oligomerization, not fibrillization, is a shared property of both alpha-synuclein mutations linked to early-onset Parkinson's disease: implications for pathogenesis and therapy. Proc Natl Acad Sci USA 97:571–576.
16. Di Pasquale E, Fantini J, Chahinian H, Maresca M, Taieb N, Yahi N. Altered ion channel formation by the Parkinson's-disease-linked E46K mutant of alpha-synuclein is corrected by GM3 but not by GM1 gangliosides. J Mol Biol 397:202–218.
17. Fredenburg RA, Rospigliosi C, Meray RK, Kessler JC, Lashuel HA, Eliezer D, and Lansbury PT, Jr. (2007) The impact of the E46K mutation on the properties of alpha-synuclein in its monomeric and oligomeric states. Biochemistry 46:7107–7118.
18. Greenbaum EA, Graves CL, Mishizen-Eberz AJ, Lupoli MA, Lynch DR, Englander SW, Axelsen PH, Giasson BI (2005) The E46K mutation in alpha-synuclein increases amyloid fibril formation. J Biol Chem 280:7800–7807.
19. Heise H, Celej MS, Becker S, Riedel D, Pelah A, Kumar A, Jovin TM, Baldus M (2008) Solid-state NMR reveals structural differences between fibrils of wild-type and disease-related A53T mutant alpha-synuclein. J Mol Biol 380:444–450.
20. Li J, Uversky VN, Fink AL (2001) Effect of familial Parkinson's disease point mutations A30P and A53T on the structural properties, aggregation, and fibrillation of human alpha-synuclein. Biochemistry 40:11604–11613.
21. Narhi L, Wood SJ, Steavenson S, Jiang Y, Wu GM, Anafi D, Kaufman SA, Martin F, Sitney K, Denis P, Louis JC, Wypych J, Biere AL, Citron M (1999) Both familial Parkinson's disease mutations accelerate alpha-synuclein aggregation. J Biol Chem 274:9843–9846.
22. Ulmer TS, Bax A (2005) Comparison of structure and dynamics of micelle-bound human alpha-synuclein andParkinson disease variants. J Biol Chem 280:43179–43187.
23. van Raaij ME, Segers-Nolten IM, Subramaniam V (2006) Quantitative morphological analysis reveals ultrastructural diversity of amyloid fibrils from alpha-synuclein mutants. Biophys J 91:L96–98.
24. Celej MS, Caarls W, Demchenko AP, Jovin TM (2009) A triple-emission fluorescent probe reveals distinctive amyloid fibrillar polymorphism of wild-type alpha-synuclein and its familial Parkinson's disease mutants. Biochemistry 48:7465–7472.
25. Bertoncini CW, Jung YS, Fernandez CO, Hoyer W, Griesinger C, Jovin TM, Zweckstetter M (2005) Release of long-range tertiary interactions potentiates aggregation of natively unstructured alpha-synuclein. Proc Natl Acad Sci USA 102:1430–1435.
26. Dedmon MM, Lindorff-Larsen K, Christodoulou J, Vendruscolo M, Dobson CM (2005) Mapping long-range interactions in alpha-synuclein using spin-label NMR and ensemble molecular dynamics simulations. J Am Chem Soc 127:476–477.
27. Chandra S, Chen X, Rizo J, Jahn R, Sudhof TC (2003) A broken alpha -helix in folded alpha -Synuclein. J Biol Chem 278:15313–15318.
28. Eliezer D, Kutluay E, Bussell R, Jr., Browne G (2001) Conformational properties of alpha-synuclein in its free and lipid-associated states. J Mol Biol 307:1061–1073.
29. George JM, Jin H, Woods WS, Clayton DF (1995) Characterization of a novel protein regulated during the critical period for song learning in the zebra finch. Neuron 15:361–372.
30. Vilar M, Chou HT, Luhrs T, Maji SK, Riek-Loher D, Verel R, Manning G, Stahlberg H, Riek R (2008) The fold of alpha-synuclein fibrils. Proc Natl Acad Sci USA 105:8637–8642.
31. Heise H, Hoyer W, Becker S, Andronesi OC, Riedel D, Baldus M (2005) Molecular-level secondary structure, polymorphism, and dynamics of full-length alpha-synuclein fibrils studied by solid-state NMR. Proc Natl Acad Sci USA 102:15871–15876.
32. Kloepper KD, Hartman KL, Ladror DT, Rienstra CM (2007) Solid-state NMR spectroscopy reveals that water is nonessential to the core structure of alpha-synuclein fibrils. J Phys Chem B 111:13353–13356.
33. Del Mar C, Greenbaum EA, Mayne L, Englander SW, Woods VL, Jr. (2005) Structure and properties of alpha-synuclein and other amyloids determined at the amino acid level. Proc Natl Acad Sci USA 102:15477–15482.
34. Chen M, Margittai M, Chen J, Langen R (2007) Investigation of alpha-synuclein fibril structure by site-directed spin labeling. J Biol Chem 282:24970–24979.
35. Krishna MM, Hoang L, Lin Y, Englander SW (2004) Hydrogen exchange methods to study protein folding. Methods 34:51–64.
36. Elbayed K, Dillmann B, Raya J, Piotto M, Engelke F (2005) Field modulation effects induced by sample spinning: application to high-resolution magic angle spinning NMR. J Magn Reson 174:2–26.
37. Paleologou KE, Schmid AW, Rospigliosi CC, Kim HY, Lamberto GR, Fredenburg RA, Lansbury PT, Jr., Fernandez CO, Eliezer D, Zweckstetter M, Lashuel HA. (2008) Phosphorylation at Ser-129 but not the phosphomimics S129E/D inhibits the fibrillation of alpha-synuclein. J Biol Chem 283:16895–16905.
38. Uversky VN, Yamin G, Munishkina LA, Karymov MA, Millett IS, Doniach S, Lyubchenko YL, Fink AL (2005) Effects of nitration on the structure and aggregation of alpha-synuclein. Brain Res Mol Brain Res 134:84–102.
39. Hoshino M, Katou H, Yamaguchi K, Goto Y (2007) Dimethylsulfoxide-quenched hydrogen/deuterium exchange method to study amyloid fibril structure. Biochim Biophys Acta 1768:1886–1899.
40. Baldwin RL (2008) The search for folding intermediates and the mechanism of protein folding. Annu Rev Biophys 37:1–21.

41. Englander SW (2006) Hydrogen exchange and mass spectrometry: A historical perspective. J Am Soc Mass Spectrom 17:1481–1489.
42. Hoshino M, Katou H, Hagihara Y, Hasegawa K, Naiki H, Goto Y (2002) Mapping the core of the beta(2)-microglobulin amyloid fibril by H/D exchange. Nat Struct Biol 9:332–336.
43. Ippel JH, Olofsson A, Schleucher J, Lundgren E, Wijmenga SS (2002) Probing solvent accessibility of amyloid fibrils by solution NMR spectroscopy. Proc Natl Acad Sci USA 99:8648–8653.
44. Miake H, Mizusawa H, Iwatsubo T, Hasegawa M (2002) Biochemical characterization of the core structure of alpha-synuclein filaments. J Biol Chem 277:19213–19219.
45. Der-Sarkissian A, Jao CC, Chen J, Langen R (2003) Structural organization of alpha-synuclein fibrils studied by site-directed spin labeling. J Biol Chem 278: 37530–37535.
46. Kloepper KD, Zhou DH, Li Y, Winter KA, George JM, Rienstra CM (2007) Temperature-dependent sensitivity enhancement of solid-state NMR spectra of alpha-synuclein fibrils. J Biomol NMR 39:197–211.
47. Iwai A, Yoshimoto M, Masliah E, Saitoh T (1995) Non-A beta component of Alzheimer's disease amyloid (NAC) is amyloidogenic. Biochemistry 34:10139–10145.
48. el-Agnaf OM, Irvine GB (2002) Aggregation and neurotoxicity of alpha-synuclein and related peptides. Biochem Soc Trans 30:559–565.
49. Giasson BI, Murray IV, Trojanowski JQ, Lee VM (2001) A hydrophobic stretch of 12 amino acid residues in the middle of alpha-synuclein is essential for filament assembly. J Biol Chem 276:2380–2386.
50. Tompa P (2009) Structural disorder in amyloid fibrils: its implication in dynamic interactions of proteins. Febs J 276:5406–5415.
51. Karpinar DP, Balija MB, Kugler S, Opazo F, Rezaei-Ghaleh N, Wender N, Kim HY, Taschenberger G, Falkenburger BH, Heise H, Kumar A, Riedel D, Fichtner L, Voigt A, Braus GH, Giller K, Becker S, Herzig A, Baldus M, Jackle H, Eimer S, Schulz JB, Griesinger C, Zweckstetter M (2009) Pre-fibrillar alpha-synuclein variants with impaired beta-structure increase neurotoxicity in Parkinson's disease models. Embo J 28: 3256–3268.
52. Kahle PJ (2008) alpha-Synucleinopathy models and human neuropathology: similarities and differences. Acta Neuropathol 115:87–95.
53. Hoyer W, Antony T, Cherny D, Heim G, Jovin TM, Subramaniam V (2002) Dependence of alpha-synuclein aggregate morphology on solution conditions. J Mol Biol 322:383–393.
54. Delaglio F, Grzesiek S, Vuister GW, Zhu G, Pfeifer J, Bax A (1995) NMRPipe: a multidimensional spectral processing system based on UNIX pipes. J Biomol NMR 6:277–293.
55. Panchal SC, Bhavesh NS, Hosur RV (2001) Improved 3D triple resonance experiments, HNN and HN(C)N, for HN and 15N sequential correlations in (13C, 15N) labeled proteins: application to unfolded proteins. J Biomol NMR 20:135–147.